CORE
Metadata, citation and similar papers at core.ac.uk
Provided by idUS. Depósito de Investigación Universidad de Sevilla

Scattering of the Halo Nucleus ^{11}Be on ^{197}Au at Energies around the Coulomb Barrier

V. Pesudo,[1,2,3] M. J. G. Borge,[1,4] A. M. Moro,[5] J. A. Lay,[6,7] E. Nácher,[1] J. Gómez-Camacho,[5,8] O. Tengblad,[1] L. Acosta,[9] M. Alcorta,[10] M. A. G. Alvarez,[11] C. Andreoiu,[12] P. C. Bender,[13] R. Braid,[14] M. Cubero,[1,15] A. Di Pietro,[16] J. P. Fernández-García,[5,17,16] P. Figuera,[18] M. Fisichella,[18] B. R. Fulton,[19] A. B. Garnsworthy,[13] G. Hackman,[13] U. Hager,[20] O. S. Kirsebom,[13,21] K. Kuhn,[14] M. Lattuada,[18,22] G. Marquínez-Durán,[23] I. Martel,[23] D. Miller,[13] M. Moukaddam,[13] P. D. O'Malley,[14] A. Perea,[1] M. M. Rajabali,[13] A. M. Sánchez-Benítez,[23] F. Sarazin,[14] V. Scuderi,[18] C. E. Svensson,[24] C. Unsworth,[13] and Z. M. Wang[25,13]

[1]*Instituto de Estructura de la Materia, CSIC, 28006 Madrid, Spain*
[2]*Department of Physics, University of the Western Cape, P/B X17, Bellville ZA-7535, South Africa*
[3]*iThemba LABS, Somerset West 7129, South Africa*
[4]*ISOLDE-EP, CERN, CH-1211 Geneva 23, Switzerland*
[5]*Departamento de FAMN, Universidad de Sevilla, 41080 Sevilla, Spain*
[6]*Dipartimento di Fisica e Astr. "Galileo Galilei", Univ. di Padova, 35131 Padova, Italy*
[7]*INFN, Sezione di Padova, via Marzolo, 8, 35131 Padova, Italy*
[8]*CN de Aceleradores (U. Sevilla, J. Andalucía, CSIC), 41092 Sevilla, Spain*
[9]*Instituto de Física, Universidad Nacional Autónoma de México, A.P. 20-364, Cd.Mx. 01000 Mexico*
[10]*Physics Division, Argonne National Laboratory, Argonne, Illinois 60439, USA*
[11]*Instituto de Física, Universidade de São Paulo, 05508-090 São Paulo, Brazil*
[12]*Department of Chemistry, Simon Fraser University, Burnaby, British Columbia, Canada V5A 1S6*
[13]*TRIUMF, 4004 Wesbrook Mall, Vancouver, British Columbia V6T 2A3, Canada*
[14]*Physics Department, Colorado School of Mines, Golden, Colorado 80401, USA*
[15]*CICANUM, Universidad de Costa Rica, Apdo. 2060 San José, Costa Rica*
[16]*Laboratori Nazionali del Sud, INFN, via Santa Sofia 62, 95123 Catania, Italy*
[17]*CN de Aceleradores (U. Sevilla, J. Andalucía, CSIC), 41092 Sevilla, Spain*
[18]*Laboratori Nazionali del Sud, INFN, via Santa Sofia 62, 95123 Catania, Italy*
[19]*Department of Physics, University of York, YO 10 5DD Heslington, York, United Kingdom*
[20]*National Superconducting Cyclotron Laboratory, Michigan State University, East Lansing, Michigan 48824, USA*
[21]*Department of Physics and Astronomy, Aarhus University, 8000 Aarhus, Denmark*
[22]*Dipartimento di Fisica e Astronomia, via Santa Sofia 64, 95123 Catania, Italy*
[23]*Departamento de Ciencias integradas, Universidad de Huelva, 21071 Huelva, Spain*
[24]*Department of Physics. University of Guelph, Guelph, Ontario N1G 2W1, Canada*
[25]*Department of Chemistry, Simon Fraser University, Burnaby, British Columbia, Canada V5A 1S6*

(Received 15 June 2016; revised manuscript received 23 January 2017; published 12 April 2017)

Angular distributions of the elastic, inelastic, and breakup cross sections of the halo nucleus ^{11}Be on ^{197}Au were measured at energies below ($E_{\rm lab} = 31.9$ MeV) and around (39.6 MeV) the Coulomb barrier. These three channels were unambiguously separated for the first time for reactions of ^{11}Be on a high-Z target at low energies. The experiment was performed at TRIUMF (Vancouver, Canada). The differential cross sections were compared with three different calculations: semiclassical, inert-core continuum-coupled-channels and continuum-coupled-channels ones with including core deformation. These results show conclusively that the elastic and inelastic differential cross sections can only be accounted for if core-excited admixtures are taken into account. The cross sections for these channels strongly depend on the $\mathcal{B}(E1)$ distribution in ^{11}Be, and the reaction mechanism is sensitive to the entanglement of core and halo degrees of freedom in ^{11}Be.

DOI: 10.1103/PhysRevLett.118.152502

Halo nuclei are very challenging systems to test our understanding of nuclear physics. Their structure is induced by the presence of very weakly bound protons or neutrons in low ℓ orbits, giving rise to a diffuse matter distribution. Reactions of halo nuclei at energies around the Coulomb barrier [1–9] unveil the importance of the structure of halo nuclei in the dynamics of the reaction process. Their weakly bound nucleons provide insight into degrees of freedom connected to slow processes. The characteristic time of motion of a weakly bound nucleon, with binding energy $B \sim 0.5$ MeV, is $\tau = \hbar/B \simeq 1.3 \times 10^{-21}$ s, to be compared with usual values, $B \sim 8$ MeV and $\tau = 8 \times 10^{-23}$ s.

Published by the American Physical Society under the terms of the Creative Commons Attribution 3.0 License. Further distribution of this work must maintain attribution to the author(s) and the published article's title, journal citation, and DOI.

The study of these relatively large time scales can be performed by means of Coulomb-dominated collisions with high-Z targets, for which the collision time $\tau = R/v$ is of the order of 10^{-21} s (using the classical distance of closest approach for a head-on collision). Halo degrees of freedom are excited by the dipole Coulomb interaction that pulls apart the neutron(s) and the core. At large projectile-target separations (i.e., small scattering angles), nuclear forces and higher Coulomb multipoles play a less significant role. Hence, the structure property that will be most relevant in a Coulomb-dominated collision is the $\mathcal{B}(E1)$ distribution.

Following this rationale, we explored in a series of experiments the scattering of ^{6}He and ^{11}Li on lead [2,3,6,8]. These nuclei do not have any bound excited state, so any excitation of the projectile will lead to its breakup, which will therefore be the dominant reaction channel. The ^{11}Li study [6,8] revealed a close relation between the $\mathcal{B}(E1)$ distribution and the breakup cross section at forward scattering angles. Nevertheless, the obtained $\mathcal{B}(E1)$ had significant discrepancies with previous Coulomb breakup measurements [10]. This result raises doubts on the consistency of the structure properties extracted from reaction data at different energy regimes. In order to address this issue, we have undertaken a new experiment, focusing this time on ^{11}Be.

Since ^{11}Be is a one-neutron halo nucleus, its theoretical treatment should be simpler as compared to the Borromean systems ^{6}He and ^{11}Li. Moreover, its $\mathcal{B}(E1)$ distribution has been extracted in several Coulomb dissociation experiments [11–14] which, although similar in shape, differ significantly in their magnitude. Finally, the peculiar properties of ^{11}Be are expected to give rise to interesting phenomena in low-energy collisions with heavy targets, particularly at near-barrier energies.

The low-lying spectrum of ^{11}Be is relatively well known [15]. It has only two bound states, the ground state (g.s.) ($1/2^{+}$) and a bound excited state at 320 keV excitation energy ($1/2^{-}$). The g.s. is known to contain admixtures of s and d neutron configurations, with the latter associated with excited components of the ^{10}Be core. Furthermore, the bound excited $1/2^{-}$ state shows the largest measured $\mathcal{B}(E1)$ between bound states [16].

This Letter reports on the first measurement of the scattering of the halo nucleus ^{11}Be on ^{197}Au at $E_{\rm lab} = 31.9$ MeV ($E_{\rm c.m.} = 29.6$ MeV) and $E_{\rm lab} = 39.6$ MeV ($E_{\rm c.m.} = 37.1$ MeV), which are, respectively, below and around the Coulomb barrier ($V_b \simeq 40$ MeV).

The challenge in this work is threefold: 1) to measure elastic, inelastic, and breakup cross sections for ^{11}Be on a high-Z target at energies near the Coulomb barrier for the first time, 2) to calculate them consistently in a strongly coupled Coulomb-dominated situation, taking into account all continuum excitations entangled with the core, and 3) to disentangle the role played by the relevant degrees of freedom of ^{11}Be in the reaction mechanism to safely correlate cross sections at low energies with $\mathcal{B}(E1)$ distributions.

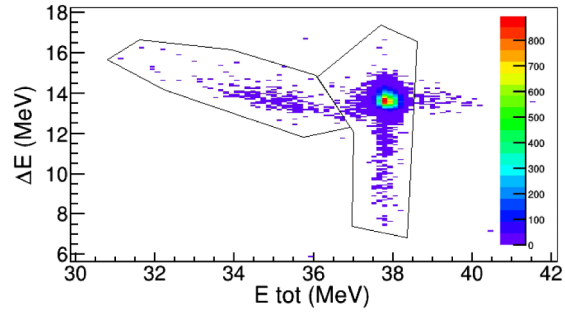

FIG. 1. Two-dimensional ΔE–$E_{\rm tot}$ spectrum of the ^{11}Be + ^{197}Au reaction at $E_{\rm lab} = 39.6$ MeV for a single pixel at $\theta_{\rm lab} = 18°$. The dominant feature corresponds to quasielastic, while the other locus corresponds to the ^{10}Be fragments detected after the breakup.

Experiment and data analysis.—The experiment was performed at TRIUMF-ISAC. The ^{11}Be beam was produced by the ISOL method. The beam purity of ^{11}Be was enhanced using the TRIUMF Laser Ionization Source (TRILIS). A mass-separated beam of ^{11}Be was delivered to the experiment with an intensity of 10^5 pps.

The target thickness was 1.9 mg/cm^2. Three telescopes (T1–T3), consisting of a 40 μm double-sided Si strip detector (DSSSD) and a 500 μm Si pad, covered angles from 14° to 97°. The fourth telescope (T4, 102°–157°) had a 20 μm single-sided strip detector and a 300 μm DSSSD.

The coincidence between the vertical and horizontal strips results in 3×3 mm^2 pixels, each subtending angles around 3°. Thus, the setup provides both a good identification of the ejectiles and adequate resolution in the scattering angle.

Surrounding the reaction chamber with the Si-detectors were twelve high-purity germanium clovers of TIGRESS [17] at a target-to-detector distance of 14.5 cm. Each clover consists of four eightfold segmented crystals in a common cryostat, surrounded by a bismuth germanate (BGO) Compton-suppression shield. Eight clovers were positioned

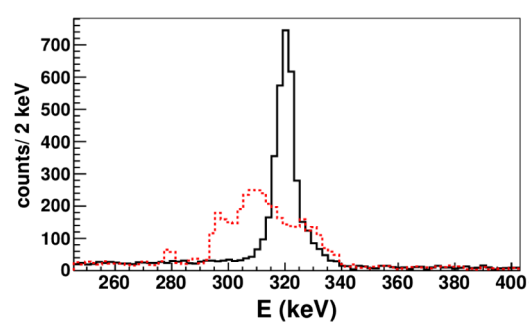

FIG. 2. γ-ray spectrum measured in TIGRESS in coincidence with the forwardmost telescope (14°–43°). Dashed red line: Doppler-shifted spectrum. Black line: Doppler-corrected spectrum for ^{11}Be recoil.

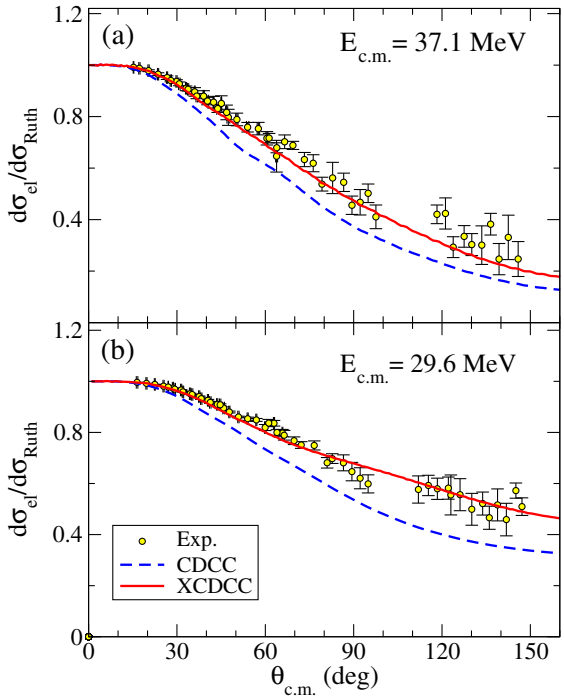

FIG. 3. Measured differential elastic scattering cross section at (a) $E_{\mathrm{c.m.}} = 37.1$ MeV and (b) 29.6 MeV, compared with the CDCC and XCDCC calculations described in the text.

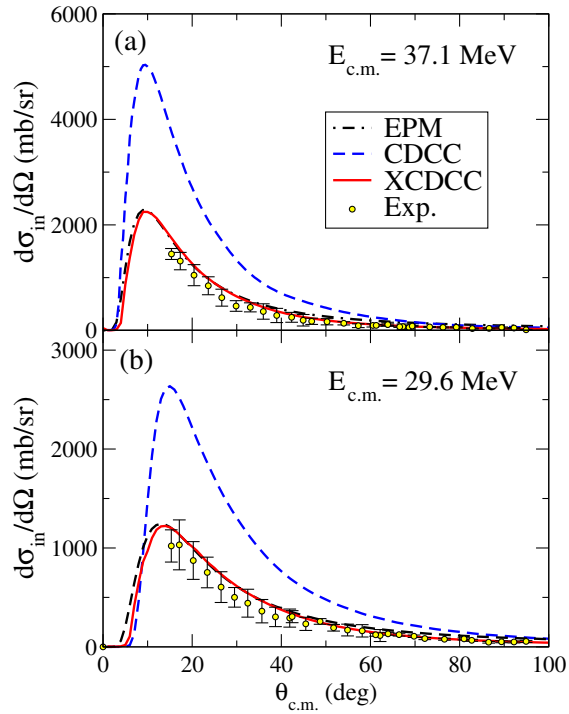

FIG. 4. Measured and calculated angular distribution of the inelastic differential cross section of $^{11}\mathrm{Be} + {}^{197}\mathrm{Au}$, populating the $1/2^-$ bound excited state in ^{11}Be for (a) $E_{\mathrm{c.m.}} = 37.1$ MeV and (b) 29.6 MeV. The curves are the EPM, CDCC, and XCDCC calculations described in the text.

at $\theta_{\mathrm{lab}} = 90°$ and four at $\theta_{\mathrm{lab}} = 135°$. In this experiment, the full photopeak efficiency for the 320 keV gamma ray was 0.121(5).

The identification of the breakup events requires the separation of the ^{10}Be and ^{11}Be fragments (see Fig. 1). This separation was accomplished in the full angular range. The large amount of breakup events observed at forward angles for reactions well below the Coulomb barrier is remarkable.

The inelastic scattering events were identified by gating the ^{11}Be events on the 320 keV γ-ray peak. Figure 2 shows the gamma-ray spectrum in the region of interest, where the 279 keV γ line, corresponding to the Coulomb excitation of the ^{197}Au target, and the 320 keV γ line, emitted after populating the bound excited state in ^{11}Be, are clearly separated. High-resolution γ-ray detectors and high granularity in the detection of charged particles and γ rays were necessary for Doppler correction of the gamma ray emitted in flight. The Compton background contribution was measured gating at the higher-energy side of the 320 keV γ-ray peak to avoid coincidences with the ^{197}Au γ line.

The events were selected by requiring a hit in any telescope and that the energy difference between both sides of the DSSSD was less than 200 keV. An angular binning of 3° was chosen for the analysis, and the centroid of each angular bin was calculated as the weighted average of the centroid of the pixels within the bin. As shown in Fig. 1, there were enough statistics in the elastic and breakup channels to evaluate the cross sections pixel by pixel. The inelastic scattering cross sections, however, are obtained by adding together the statistics of pixels within the same angular bin. The angular distributions of the elastic, inelastic, and breakup channels are shown in Figs. 3, 4, and 5, respectively. Beyond 100°, inelastic and breakup events were observed, but their small statistics prevented us from extracting reliable cross sections. It is remarkable that even at energies below the barrier, there is a significant deviation of the elastic channel with respect to Rutherford scattering (Fig. 3), even at very forward angles (50° is a lower limit for the grazing angle), corresponding to very distant trajectories. This is a clear signature of dipole polarizability [18].

Theoretical analysis.—The structure of ^{11}Be (ground state, excited state, and continuum states) is described using two models. First, a single particle model (SP), which ignores the structure of the ^{10}Be core and describes the motion of the halo neutron using a mean-field potential of Woods-Saxon type that reproduces the neutron separation energies of the $1/2^+$ g.s. and the $1/2^-$ excited state [19]. The second is a particle-plus-core model (CEX), which takes into account the g.s. (0^+) and first excited state (2_1^+) in ^{10}Be. The potential parameters for this model are taken from Ref. [20]. The interaction of the halo neutron with the core has a quadrupole deformation given by $\beta = 0.67$ [21]. Both models yield similar total $\mathcal{B}(E1)$ strengths because both have similar rms radii for the halo neutron in the g.s.

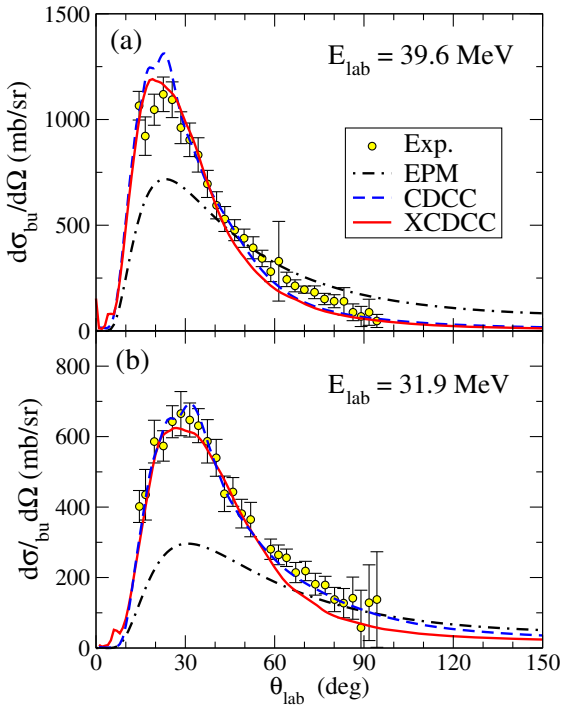

FIG. 5. Experimental differential breakup cross section in the laboratory frame at (a) $E_{\rm lab} = 39.6$ MeV and (b) 31.9 MeV, compared with EPM, CDCC, and XCDCC calculations described in the text.

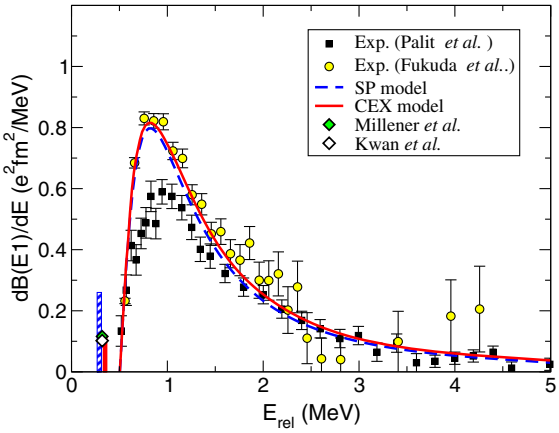

FIG. 6. Experimental and calculated $\mathcal{B}(E1)$ strength distributions for ^{11}Be. The experimental distributions are from the Coulomb dissociation experiments of Refs. [12,14]. The filled diamond and the vertical bars represent the experimental and calculated $\mathcal{B}(E1; 1/2^+ \to 1/2^-)$ value (in $e^2\,\mathrm{fm}^2$) between the bound states of ^{11}Be [16,25]. The theoretical distributions correspond to the SP and CEX models.

In the CEX model, the $\mathcal{B}(E1)$ to the continuum exceeds that of the SP model by 0.14 $e^2\,\mathrm{fm}^2$, but both are compatible with the Coulomb dissociation data of Ref. [12] (see Fig. 6). Conversely, the $\mathcal{B}(E1)$ for the $1/2^-$ bound state is larger in the SP model by this same amount, and this results in an overestimation of the experimental value for this state. The inclusion of the core deformation (CEX) reduces the $\mathcal{B}(E1)$ to the bound state, shifting it to the continuum and resulting in a good agreement of both strengths. This is due to the fact that the admixture of the core excitation components in the $1/2^+$ and $1/2^-$ states reduces significantly the $E1$ matrix elements. The CEX model presented in this work gives for the ^{11}Be g.s., 88% of ^{10}Be (0^+) and 12% of ^{10}Be (2^+). Although the s-wave content is somewhat higher than that extracted from some transfer [22] and Coulomb dissociation experiments [12], it is consistent with recent *ab initio* calculations [23].

The scattering observables are calculated using three models. Firstly, the equivalent photon method (EPM) [24], consisting in a semiclassical calculation with Coulomb trajectories and pure first order $E1$ excitation of the ^{11}Be projectile due to the Coulomb interaction with the target. In this model, inelastic cross sections are proportional to the $\mathcal{B}(E1)$ to the $1/2^-$ bound state. Breakup cross sections are proportional to a certain integral of the $\mathcal{B}(E1)$ distribution to the continuum, which is dominated by breakup energies close to the threshold. Secondly, the continuum-discretized coupled-channels (CDCC) calculation [26], using as a structure model the SP model described above. It takes into account the dynamical effect of the halo degree of freedom on the dynamics of the collision. Finally, the extended continuum-discretized coupled-channels calculation (XCDCC) [27], which uses the CEX model and takes into account both the halo and core degrees of freedom. Convergence of the studied observables for the CDCC and XCDCC calculations required a very large model space ($J^\pi \leq 15/2^\pm$ and $E_x < 12$ MeV for the total angular momentum and excitation energy of ^{11}Be) and also narrow energy bins ($\delta E \simeq 140$ keV) at energies close to the threshold. Coulomb dipole continuum-continuum couplings, which go well beyond the first order, are essential to get converged results.

Discussion.—Coulomb breakup processes populate mostly the low energy continuum of ^{11}Be which, according to Fig. 6, mainly involves excitation energies below 3 MeV, dominated by a maximum around $E_x \simeq 1$ MeV. In a Coulomb dissociation experiment performed at RIKEN [12] ($E/A = 70$ MeV, $\theta_{\rm c.m.} \simeq 5°$), the collision time (defined as the ratio of the distance of closest approach to the velocity) is $\tau_{\rm coll} \simeq (0.5 - 1.0) \times 10^{-22}$ s. This time is short compared to the characteristic time for the excitation of the relevant Coulomb breakup states $\tau_{\rm ex} = \hbar/E_x(1\ \mathrm{MeV}) = 6 \times 10^{-22}$ s or the characteristic time of the deformation in ^{10}Be, $\tau_d = \hbar/E(2^+, {}^{10}\mathrm{Be}) = 2 \times 10^{-22}$ s. This means that, during the collision, the charge distribution of the ^{11}Be g.s. wave function remains *frozen*. In this case of fast collisions, the breakup reaction will essentially be a first order process, and the breakup cross sections will be proportional to the $\mathcal{B}(E1)$ distribution, determined by $M(E1)$ matrix elements coupling ^{11}Be g.s. with its continuum states. Under these

conditions, there will not be a sizeable distortion of ^{11}Be under the Coulomb field of the target. This assumption justifies the use of the EPM to obtain $\mathcal{B}(E1)$ distributions directly from breakup cross sections at intermediate scattering energies.

The dynamical situation of the present experiment is very different ($E \simeq 35$ MeV, $\theta_{\mathrm{c.m.}} = 13°$–$150°$). The collision time, $\tau_{\mathrm{coll}} \simeq (5\text{–}10) \times 10^{-22}$ s, is large enough to let the ^{11}Be charge distribution readapt during the collision. In this slow breakup scenario, the assumptions leading to the EPM are no longer valid, and one requires a proper description of the scattering which takes into account the distortion of ^{11}Be continuum wave functions. This is done in the CDCC calculation, which takes into account the coupling of the halo degrees of freedom, and in the XCDCC calculation, which takes into account the coupling to both the halo and the core degrees of freedom. As the collision is slow, there is the possibility of multiple Coulomb excitation, which is manifested in the need to include high angular momenta in the continuum. Also, to describe accurately continuum to continuum couplings, the energy interval of the most relevant bins should be about $\delta E < \hbar/\tau_{\mathrm{coll}} \simeq 600$ keV, which is fulfilled in our calculation.

Now, we can interpret the results of breakup cross sections (Fig. 5). The EPM model [based on the $\mathcal{B}(E1)$ distribution] largely underestimates the breakup cross section in the range which is safely Coulomb dominated ($\theta_{\mathrm{c.m.}} < 50°$). This indicates that there is a distortion of ^{11}Be during the slow collision, which then breaks up more efficiently than in the first order mechanism. The CDCC calculation, based on a SP model that reproduces the $\mathcal{B}(E1)$ distribution, reproduces the breakup cross sections. This indicates that the complex dynamics of the slow breakup is well described by properly taking into account the halo degrees of freedom, included in CDCC. Regarding the XCDCC calculation, it is based in a CEX model with the appropriate admixture of 0^+ and 2^+ components and with the adequate noncentral interaction that reproduces simultaneously the $\mathcal{B}(E1)$ to the continuum and to the $1/2^-$ bound state. XCDCC reproduces elastic, inelastic, and breakup cross sections, indicating that the model is able to describe the dynamical evolution in a slowly varying Coulomb field.

In the case of inelastic scattering (Fig. 4), as opposed to breakup, both the initial and final states are bound and discrete. Thus, the role of distortion is not as important as in the breakup cross sections. Hence, the EPM gives, in the Coulomb-dominated regime, similar results to those obtained with the more sophisticated XCDCC, as both start from similar $\mathcal{B}(E1)$ values. Interestingly, these calculations overestimate the data by ~14%, suggesting that the $\mathcal{B}(E1; 1/2^+ \to 1/2^-)$ value should be smaller than the lifetime value by this same amount, in accord with some Coulomb excitation experiments [16,28]. The CDCC calculation does not include 2^+ components, hence, it gives a larger $\mathcal{B}(E1)$ value and overestimates the cross sections.

Conclusions.—We have presented the elastic, inelastic, and breakup data for the $^{11}\mathrm{Be} + {}^{197}\mathrm{Au}$ reaction at energies around and below the Coulomb barrier. This corresponds to a dynamical situation in which the weakly bound projectile is exposed to a strong slowly varying Coulomb field. This study is complementary to the intermediate-energy Coulomb dissociation experiments performed at RIKEN and GSI that can be understood as exposing halo nuclei to rapidly varying Coulomb fields. The XCDCC calculations presented here describe the distortion of ^{11}Be in the Coulomb field, which includes the dynamical core polarization. The fact that only the XCDCC calculations, starting from a structure model that reproduces the experimental $\mathcal{B}(E1)$ values, also reproduce the elastic, inelastic, and breakup cross sections indicates that we have the adequate theoretical tools to analyze low energy Coulomb breakup reactions.

The results presented in this Letter validate the ^{11}Be dipole distribution obtained from the latest Coulomb dissociation experiment performed at RIKEN and open the possibility of complementing high energy Coulomb breakup experiments with low energy ones with the purpose of learning not only about the $\mathcal{B}(E1)$ distribution of halo nuclei, but also about the dynamics of the halo nuclei in a strong Coulomb field.

This work has been supported by the Spanish Ministerio de Economía y Competitividad and FEDER, under the Projects No. FPA2015-64969-P, No. FIS2014-53448-C2-1-P, No. FPA2013-47327-c02-01-R, No. FPA2012-32443, No. FIS2013-41994-P, and Consolider CPAN CSD2007-00042; the EUROCORES Project No. EUI-2009-04162; the European Unions Horizon 2020 research and innovation program under Grant Agreement No. 654002; the Helmholtz Association (HGT) through the Nuclear Astrophysics Virtual Institute (VH-VI-417); ATI Sistemas; The Natural Sciences and Engineering Research Council of Canada; The Canada Foundation for Innovation; and the British Columbia Knowledge Development Fund. TRIUMF receives federal funding via a contribution agreement through the National Research Council of Canada. The research leading to these results has received funding from the European Commission, Seventh Framework Program (FP7/2007-2013) under Grant Agreement No. 600376. J. A. L. is a Marie Curie Piscopia fellow at the University of Padova. O. S. K. acknowledges support from the Villum Foundation.

[1] M. Mazzocco *et al.*, Eur. Phys. J. A **28**, 295 (2006).
[2] D. Escrig *et al.*, Nucl. Phys. **A792**, 2 (2007).
[3] A. M. Sánchez-Benítez *et al.*, Nucl. Phys. **A803**, 30 (2008).
[4] L. Acosta *et al.*, Eur. Phys. J. A **42**, 461 (2009).
[5] L. Acosta *et al.*, Phys. Rev. C **84**, 044604 (2011).
[6] M. Cubero *et al.*, Phys. Rev. Lett. **109**, 262701 (2012).
[7] A. Di Pietro *et al.*, Phys. Rev. Lett. **105**, 022701 (2010); Phys. Rev. C **85**, 054607 (2012).

[8] J. P. Fernández-García *et al.*, Phys. Rev. Lett. **110**, 142701 (2013).
[9] J. P. Fernández-García *et al.*, Phys. Rev. C **92**, 044608 (2015).
[10] T. Nakamura *et al.*, Phys. Rev. Lett. **96**, 252502 (2006).
[11] T. Aumann and T. Nakamura, Phys. Scr. **T152**, 014012 (2013).
[12] N. Fukuda, T. Nakamura, N. Aoi, N. Imai, M. Ishihara, T. Kobayashi, H. Iwasaki, T. Kubo, A. Mengoni, M. Notani, H. Otsu, H. Sakurai, S. Shimoura, T. Teranishi, Y. X. Watanabe, and K. Yoneda, Phys. Rev. C **70**, 054606 (2004).
[13] T. Nakamura *et al.*, Phys. Lett. B **331**, 296 (1994).
[14] R. Palit *et al.*, Phys. Rev. C **68**, 034318 (2003).
[15] J. H. Kelley *et al.*, Nucl. Phys. **A880**, 88 (2012).
[16] E. Kwan *et al.*, Phys. Lett. B **732**, 210 (2014).
[17] G. Hackman and C. E. Svensson, Hyperfine Interact. **225**, 241 (2014).
[18] M. V. Andres and J. Gomez-Camacho, Phys. Rev. Lett. **82**, 1387 (1999).
[19] P. Capel, G. Goldstein, and D. Baye, Phys. Rev. C **70**, 064605 (2004).
[20] T. Tarutina, L. C. Chamon, and M. S. Hussein, Phys. Rev. C **67**, 044605 (2003).
[21] F. M. Nunes, J. A. Christley, I. J. Thompson, R. C. Johnson, and V. D. Efros, Nucl. Phys. **A609**, 43 (1996).
[22] S. Fortier *et al.*, Phys. Lett. B **461**, 22 (1999).
[23] A. Calci, P. Navrátil, R. Roth, J. Dohet-Eraly, S. Quaglioni, and G. Hupin, Phys. Rev. Lett. **117**, 242501 (2016).
[24] K. Alder and A. Winther, *Electromagnetic Excitation* (North-Holland, Amsterdam, 1975).
[25] D. J. Millener, J. W. Olness, E. K. Warburton, and S. S. Hanna, Phys. Rev. C **28**, 497 (1983).
[26] N. Austern, Y. Iseri, M. Kamimura, M. Kawai, G. Rawitscher, and M. Yahiro, Phys. Rep. **154**, 125 (1987).
[27] N. C. Summers, F. M. Nunes, and I. J. Thompson, Phys. Rev. C **73**, 031603 (2006); R. de Diego, J. M. Arias, J. A. Lay, and A. M. Moro, Phys. Rev. C **89**, 064609 (2014).
[28] T. Nakamura, T. Motobayashi, Y. Ando, A. Mengoni, T. Nishio, H. Sakurai, S. Shimoura, T. Teranishi, Y. Yanagisawa, and M. Ishihara, Phys. Lett. B **394**, 11 (1997).